High kinetic energy release upon dissociation and ionization of an N_2^+ beam by intense few-cycle laser pulses

B. Gaire, J. McKenna, A. M. Sayler, Nora G. Johnson, E. Parke, K. D. Carnes, B. D. Esry, and I. Ben-Itzhak
J.R. Macdonald Laboratory, Department of Physics, Kansas State University, Manhattan, Kansas 66506, USA
(Received 7 May 2008; published 25 September 2008)

The kinetic energy release (KER) and angular distribution for dissociation and ionization of N_2^+ in an intense short pulse (7 fs) laser at 790 nm was measured by employing a coincidence three-dimensional momentum imaging method that provides kinematically complete information on the dissociation. At an intensity of 6.0×10^{15} W/cm^2 a high-KER peak (~6.1 eV) unexpectedly appears in the dissociation spectrum in addition to the usual low-KER peak (~0.6 eV). Additionally, the KER distribution in ionization, which peaks around 7 eV, has a tail that surprisingly extends well beyond the Coulomb explosion energy. Both these high-KER contributions result from dissociation pathways involving highly excited states of N_2^+ with steep potential curves as indicated by the dressed state potential energy curves picture.

DOI: 10.1103/PhysRevA.78.033430 PACS number(s): 33.80.Rv, 42.50.Hz

I. INTRODUCTION

The interaction of an intense laser with diffuse matter has been explored widely in the past decade (see reviews in Refs. [1–3]). For this purpose, atoms, molecules, and molecular ions are the most common targets. The simplest molecule H_2^+ has often been used as a testing ground for both theory and experiment, since exploring the physics of this single electron system is a much less demanding task than studying a larger multielectron system. Some of the important phenomena that have been observed in these studies include bond softening (BS) [4,5], vibrational trapping (VT, also known as bond hardening) [4–6], above-threshold dissociation (ATD) [7,8], above-threshold ionization (ATI) [9,10], Coulomb explosion (CE) [11–13], and above-threshold Coulomb explosion (ATCE) [14,15].

Typically, in a strong laser field, molecular dissociation yields a kinetic energy release (KER) that is much lower than what one would expect for photodissociation. This has led to the discovery of the bond softening mechanism [4,5]. Figure 1 shows the laser-dressed diabatic $1s\sigma_g$ and $2p\sigma_u$ Born-Oppenheimer potentials of H_2^+ in what is referred to as the Floquet representation [2,6,16–19]. In this representation the up or down shift of the potential energy curves (PECs) by n times the photon energy $\pm n\omega$ corresponds to the emission or absorption of n photons, respectively, and the resulting dressed states are denoted by the state followed by the label $\pm n\omega$ in Fig. 1. This is equivalent to the alternative picture, often used, where a transition between any two states is represented by vertical up and down arrows corresponding to the absorption and emission of photons, respectively (see, e.g., Ref. [20]). For convenience we will use the dressed states picture.

On these dressed PECs in Fig. 1, the H_2^+ wave packet can make a transition at the crossings between curves governed by molecular dipole selection rules. In addition to the diabatic curves we have also shown the adiabatic curves, for which the laser-molecule coupling is included, near the crossing of the $|1s\sigma_g\text{-}0\omega\rangle$ and the $|2p\sigma_u\text{-}1\omega\rangle$ states. A wave packet near this crossing dissociates through the process of bond softening. In addition, a wave packet just above the crossing, as shown in Fig. 1, may be trapped in the shallow potential well formed above the crossing, a process appropriately named vibrational trapping.

When more than the minimum number of photons needed for dissociation are absorbed, e.g., $|2p\sigma_u\text{-}3\omega\rangle$, and dissociation occurs through this path, it is called above-threshold dissociation [7,8] (in analogy to above-threshold ionization [9,10]). A wave packet dissociating by ATD along the $|2p\sigma_u\text{-}3\omega\rangle$ state can have two pathways, i.e., it can either remain on the $|2p\sigma_u\text{-}3\omega\rangle$ curve or end up on the $|1s\sigma_g\text{-}2\omega\rangle$ curve by a transition at the next crossing between the $|1s\sigma_g\text{-}2\omega\rangle$ and $|2p\sigma_u\text{-}3\omega\rangle$ states. The latter pathway results in the reemission of a photon. A curved arrow is shown in Fig. 1 to indicate this latter transition. For both ATD pathways the KER is larger than in dissociation by the bond softening mechanism. In general, ATD has a higher KER and a lower

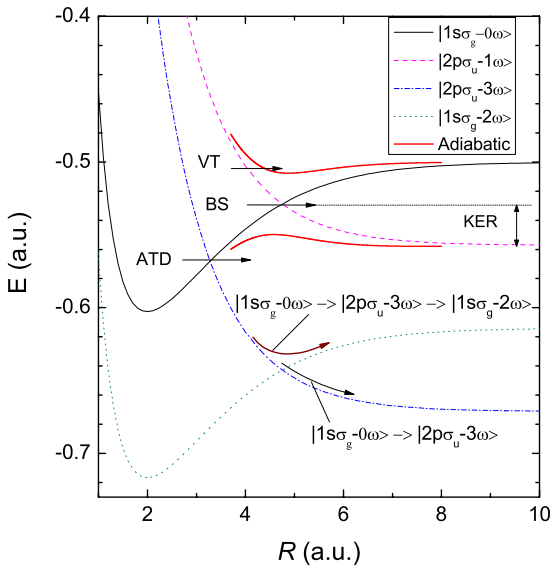

FIG. 1. (Color online) Born-Oppenheimer potentials of H_2^+, dressed by net absorbed number of photons $n\omega$. Also indicated are the vibrational trapping (VT), bond softening (BS), and above-threshold dissociation (ATD) mechanisms.

probability of occurring than BS because of the large number of photons involved.

Similar to molecular dissociation by BS, ionization typically yields lower KER than that predicted for direct ionization. This is due to enhanced ionization [21,22], i.e., higher ionization probability, for stretched molecules. This mechanism can be viewed as ionization of the molecule along its dissociation path. Moreover, similar to dissociation, ionization may also be explained using the dressed-states picture as demonstrated recently by Esry *et al.* [14]. While fundamentally this is a multiphoton interpretation (explicitly referring to photons), it is still useful even in the intensity regime where ionization would traditionally be described as occurring by electron tunneling. Indeed, as pointed out by Esry *et al.* [14], the multiphoton dressed-state picture works best near the appearance intensity for ionization where curve crossings just begin to open, and at higher intensities, the KER peaks are mostly broadened from their low intensity values. This can be viewed as a widening of the curve crossings at high intensity, just like the adiabatic curves in Fig. 1, leading to ionization over a broader range of internuclear separation R.

In this work we explore the dissociation and ionization pathways of an N_2^+ beam in intense ultrashort 790 nm laser pulses. The single and multiple ionization of N_2 molecules in a strong ~800 nm laser field has been studied experimentally by several groups (e.g., Refs. [22–30]) but never before starting from an N_2^+ beam target. In particular, we focus on an unusually high-KER feature in the dissociation into $N^+ + N$. This high-KER peak is more than 5 eV higher than a low-KER peak that has commonly been observed for N_2^+ dissociation starting from an N_2 target. The separation of the low (0.6 eV) and high (6.1 eV) KER peaks is much larger than the photon energy (1.57 eV) for 790 nm wavelength. In addition, we show that the dissociation pathways responsible for this high-KER feature lead to KER values in ionization much higher than expected for Coulomb explosion into $N^+ + N^+$. Although the intensity range covered, up to 6×10^{15} W/cm^2, spans into the tunneling regime, we find it informative to interpret the results using the Floquet picture, exemplified in Fig. 1 for H_2^+. This is because the Floquet dressed-states picture allows for clear identification of both dissociation and ionization pathways using their KER and angular distributions, as well as their intensity dependence [14].

II. EXPERIMENTAL SETUP

For the measurements of N_2^+ we have applied a coincidence three-dimensional (3D) momentum imaging method used previously for the study of the single electron systems H_2^+, HD^+, and D_2^+ [31,32], and other many-electron systems, e.g., O_2^+ [33] and ND^+ [34]. The details of our experimental setup are described in previous papers [31,32], therefore, only a brief description follows.

The molecular ion beam was generated in an electron impact ion source and accelerated to 9 keV beam energy. Magnetic and electric fields were used to guide the ion beam towards an interaction point where the laser and the collimated ion beam were crossed within an electrostatic spectrometer. At the interaction point molecular ions were dissociated or ionized by the pulsed intense laser. The transverse component of molecular breakup energy imparted to the dissociative fragments separated the fragments from the primary ion beam. These fragments were then detected using a microchannel plate delayline detector, operated in event mode, that recorded the time and position of each fragment created for every laser pulse. The primary ion beam was collected in a small on-axis Faraday cup (2 mm in diameter) and, due to blocking by the cup, fragments with KER $\lesssim$0.1 eV were lost. In the interaction region, the spectrometer electric field accelerated the charged fragments with respect to the neutral particles. Thus the fragments, ions and neutrals, were separated in time of flight, and dissociation could be clearly distinguished from ionization as illustrated in Fig. 2. In this figure we show the time of flight of the first particle to hit the detector versus the time of flight of the second particle for two breakup channels, namely, $N^+ + N$ and $N^+ + N^+$. From the position and time information recorded for both fragments, the complete 3D kinematics of the breakup events were computed [35]. That is, the kinetic energy release upon fragmentation and θ, the angle between the molecular axis and the laser polarization direction, were computed.

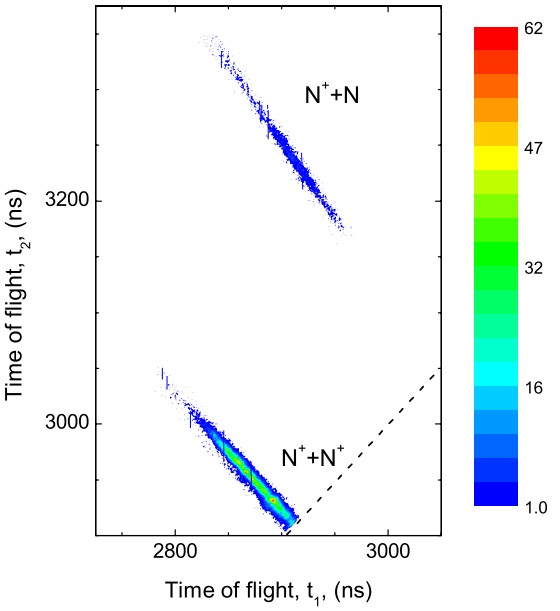

FIG. 2. (Color online) A density plot of the time of flight of the first particle (t_1) to arrive at the detector against that of the second particle (t_2), to illustrate the separation of breakup channels in our coincidence measurement. The dashed line indicates the loci $t_1 = t_2$.

The laser used in the experiment was a Ti:sapphire system (790 nm), which, following temporal compression of the pulses using a neon-filled hollow-core fiber and chirped mirror arrangement, provided linearly polarized 7 fs (full width at half maximum) pulses at 1 kHz repetition rate. These pulses were focused onto the ion beam target using an $f = 203$ mm off-axis parabolic mirror. The laser intensity at the target was varied by scanning the position of the laser focus with respect to the target. Hence, the peak intensity (6.0

$\times 10^{15}$ W/cm^2) was achieved with the ion beam crossing the center of the laser focus, and low intensity (6.5×10^{14} W/cm^2) was achieved by moving the laser focus away from the ion beam center along the laser propagation direction. This technique is known as an intensity selective scan [36,37] and takes advantage of the increased interaction volume for low intensity measurements.

The N_2^+ beam target used in these studies had some unique properties. The most important one is that it was predominantly in its electronic ground state and vibrationally cold. This follows since the ground state of N_2^+ (2.13 a.u. [38]) has a similar equilibrium distance as that of N_2 (2.08 a.u. [39]), hence there is a large Franck-Condon overlap of the ground vibrational state of N_2 with the low vibrational states of N_2^+. For the N_2^+ ions produced in an ion source by electron impact ionization of N_2 (i.e., a vertical transition), most of the population is distributed among the three lowest electronic states, namely, the ground state $X\ ^2\Sigma_g^+$ and the metastable states $A\ ^2\Pi_u$, and $B\ ^2\Sigma_u^+$ [40–42]. These states are shown in Fig. 3(a) along with some additional relevant PECs of N_2^{q+} with $q \leqslant 2$. The radiative lifetimes of the different vibrational levels of the N_2^+ metastable states are a few tens of microseconds for the $A\ ^2\Pi_u$ and a few nanoseconds for the $B\ ^2\Sigma_u^+$ [46]. So, the electronic and vibrational population distributions change from when the ions are first produced in the ion source to when they reach the interaction region, i.e., after the transit time of about 20 μs in our setup. We have calculated the overall vibrational population distribution at the interaction region by applying the method described by Crandall *et al.* [41] and using the data from Refs. [41,46]. The resulting electronic and vibrational populations of the ions in the interaction region are shown in Fig. 3(b). At the interaction time, the ground vibrational level ($v=0$) of the $X\ ^2\Sigma_g^+$ state is most highly populated (>40%), with little population remaining in the $A\ ^2\Pi_u$ state (total population <13%) and virtually no population in the $B\ ^2\Sigma_u^+$ state. Furthermore, more than 83% of the population is in $v=0-7$ of $X\ ^2\Sigma_g^+$, i.e., within less than one photon energy from the bottom of the potential well.

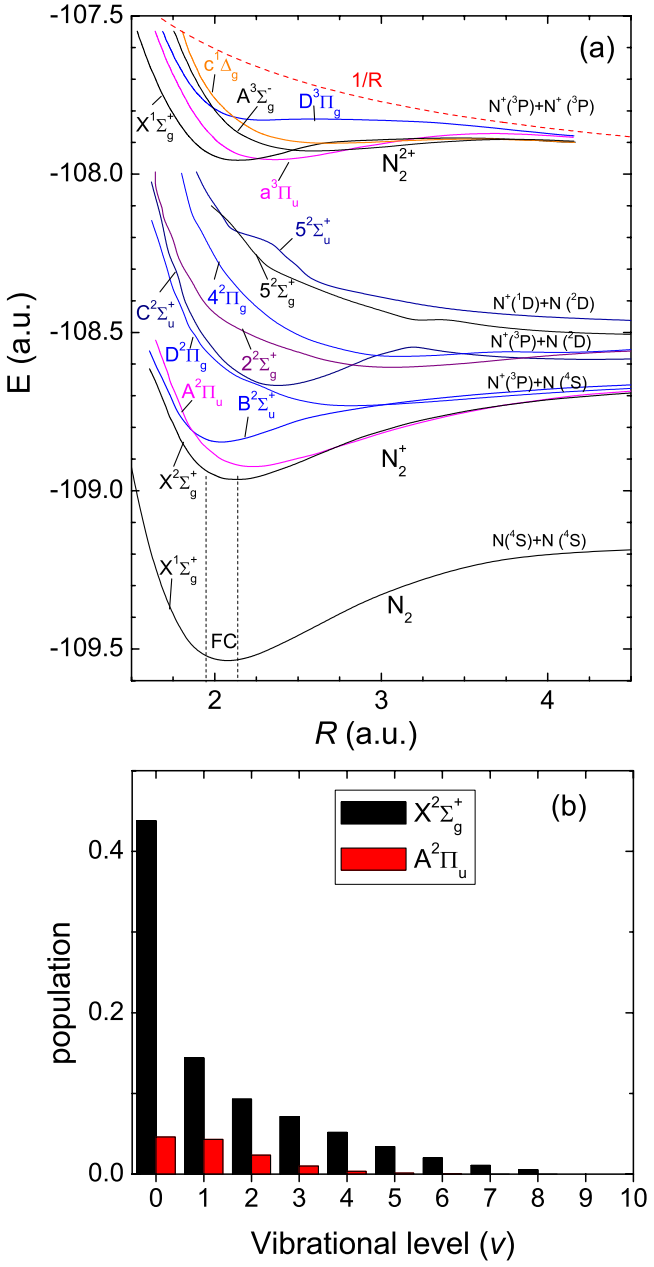

FIG. 3. (Color online) (a) A simplified potential energy curve diagram of N_2^{q+} ($q \leqslant 2$) showing only a selection of the lowest-lying curves for each q. The PEC of N_2 is taken from Ref. [39], N_2^+ from [43,44], and N_2^{2+} from Ref. [45]. The structure in some of these curves is due to avoided crossings with neighboring electronic states not shown. The dashed vertical lines represent the Franck-Condon (FC) transition region. The zero of the energy is for the fully stripped $N^{7+}+N^{7+}+14e^-$ limit. (b) Calculated vibrational population distribution of N_2^+ in the interaction region following decay of metastable states from the source (see text).

III. RESULTS AND DISCUSSION

A. Dissociation

The KER distributions for the dissociation of N_2^+ into the $N^+ + N$ channel [often referred to as the (1,0) channel] are displayed in Fig. 4. For the lower measured intensity of 6.5×10^{14} W/cm^2 [see panel (a)] the results display a sole low energy peak centered around 0.6 eV which extends up to ~2.5 eV. This peak is equivalent to that observed in other studies of N_2^+ dissociation starting with an N_2 target [25,27,28,30]. In contrast to our work, however, some of these papers report distributions peaked around 0.0 eV (for 25 fs, 10^{14} W/cm^2 pulses) [27], 1.2 eV (for 33 fs, 10^{15} W/cm^2 pulses) [25], 1.8 eV (for 55 fs, ~10^{14} W/cm^2 pulses) [28], and 0.45 eV (for 70 fs, ~10^{14} W/cm^2 pulses) [30]. The reason for these differences is unclear and further investigation is required.

By comparison, the KER spectrum measured under the same experimental conditions as Fig. 4(a) but for a higher intensity of 6.0×10^{15} W/cm^2, shown in panel (b), exhibits an additional KER peak around 6.1 eV. Such a high-KER feature is rather surprising for the dissociation of diatomic molecules such as N_2^+ and, to the best of our knowledge, has not been reported previously. It is important to note that in

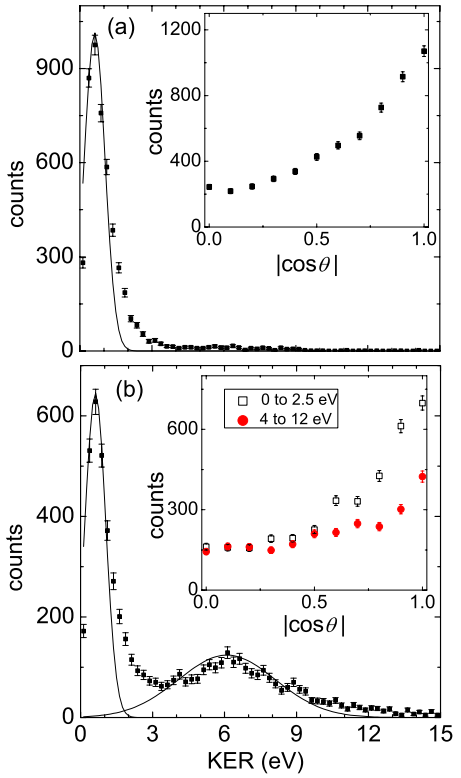

FIG. 4. (Color online) (a), (b) Measured KER distributions for dissociation of N_2^+ using 7 fs pulses at intensities (a) 6.5×10^{14} W/cm^2 and (b) 6.0×10^{15} W/cm^2 with corresponding angular distributions (inset) plotted versus $|\cos\theta|$, where θ is the angle between the molecular axis and the direction of the laser polarization. The error bars denote the statistical errors in the data. The fitted curves are Gaussian distributions centred at the peak of the measured KER distribution and are only used as a guide.

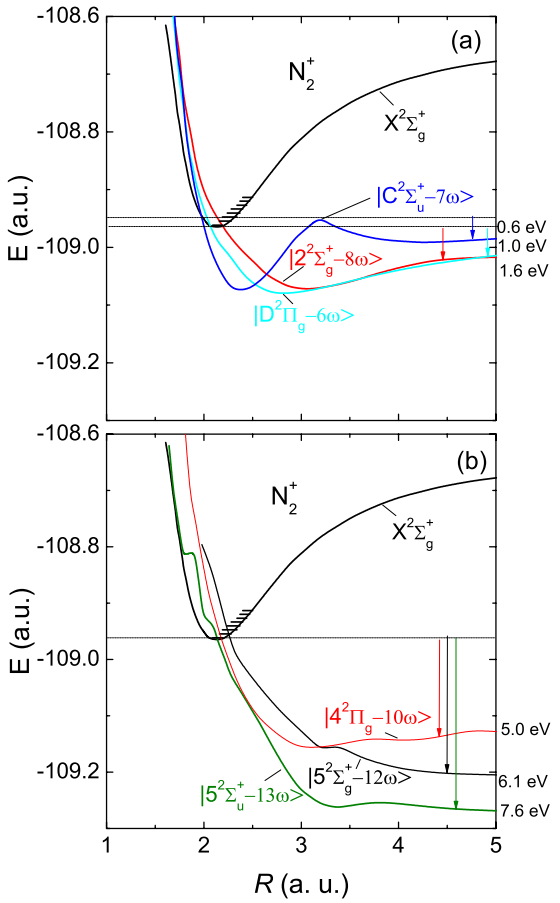

FIG. 5. (Color online) Dressed-states diabatic picture of N_2^+ illustrating dissociation pathways that lead to (a) low- and (b) high-KER dissociation (see text). The short lines within the potential well represent the different vibrational levels and the horizontal lines near the bottom of the potential represent the initial energy of the dissociation wave packet. Potential energy curves for N_2^+ have been reproduced from Ref. [44]. The structure in some of these curves is due to avoided crossings with neighboring electronic states not shown.

many previous studies only charged fragments were detected so that the breakup channels (i.e., $N^+ + N$, $N^+ + N^+$, etc.) were identified only by the KER. Therefore, high KER in $N^+ + N$ dissociation could be masked by the energetic $N^+ + N^+$ breakup. This limitation is not a problem in our method because the different breakup channels are separated through detection of both the charged and neutral fragments in coincidence as discussed briefly in Sec. II and in detail in Refs. [31,32].

Additional information on dissociation is provided by the angular distribution of the fragments as displayed in the $\cos\theta$ plots in the insets of Fig. 4 for the two different intensities discussed above. The type of the transition involved in a dissociation pathway can be found by the change in the angular momentum quantum number $\Delta\Lambda$ [33,34,47]. A parallel transition is defined by $\Delta\Lambda = 0$ (e.g., $\Sigma \leftrightarrow \Sigma$, $\Pi \leftrightarrow \Pi$) and depends on the laser field strength parallel to the molecular axis, while a perpendicular transition corresponds to $\Delta\Lambda = \pm 1$ (e.g., $\Sigma \leftrightarrow \Pi$) and depends on the laser field strength perpendicular to the molecular axis. To account for the volume element of the dissociation sphere, we bin the angular distributions as a function of $\cos\theta$ rather than θ such that an isotropic angular distribution will appear flat on a $\cos\theta$ plot. We see in the insets of Fig. 4 that the $|\cos\theta|$ distributions have significant counts along $|\cos\theta| = 0$, in addition to the major contribution along $|\cos\theta| = 1$. This implies that, in addition to the dominant parallel transitions, perpendicular transitions also play an important role in the dissociation.

1. Low-KER dissociation pathway

The mechanisms or pathways responsible for the KER and $|\cos\theta|$ features observed may be determined from close inspection of the PECs of N_2^+. We begin by focusing on the origin of the low-KER peak, which we identify as being produced by dissociation along one of the pathways shown in Fig. 5(a). By process of elimination of all other allowed dissociation paths based on the expected KER and angular distributions (see Ref. [33] for the method used), we find the following pathways to be the important ones.

The ground vibrational level of the $|X\,^2\Sigma_g^+\text{-}0\omega\rangle$ state couples to the $|D\,^2\Pi_g\text{-}6\omega\rangle$ state, dissociating to $N^+(^3P) + N(^4S)$. It is a valid even-photon gerade-gerade coupling resulting in a perpendicular transition ($\Sigma \rightarrow \Pi$) and is thus likely to be the source of the counts near $|\cos\theta| = 0$ in the

inset of Fig. 4(a). Dissociation on this state will yield a KER of about 1 eV, estimated from the difference between the initial energy of the molecule and the asymptotic limit of the dissociation state. Note, there may be a small deviation from this value due to possible Stark shifting of vibrational states, depending on the intensity. Since the main peak of the low-KER feature in Fig. 4(a) is at lower energy than that given by this pathway (i.e. this pathway contributes to the extended tail of the distribution), we look for other pathways for dissociation involving excited final products.

One strong possibility for a dissociation pathway is that the population of the N_2^+ $|X\,^2\Sigma_g^+\text{-}0\omega\rangle$ state near $v=2$ couples to the dressed $|C\,^2\Sigma_u^+\text{-}7\omega\rangle$ excited state, dissociating to the $N^+(^3P)+N(^2D)$ limit. This pathway involves a parallel transition with an odd number of photons absorbed, resulting from a gerade-ungerade coupling. One will notice that there is a barrier in this state at an internuclear distance R of about 3.2 a.u., but a wave packet dissociating from the $v=2$ state should just have enough energy to overcome this barrier and will end up with dissociation energy of 0.6 eV in good agreement with the peak of the observed distribution. Note that approximately 10% of the total fraction of the beam is in the $v=2$ vibrational level.

One other state, namely, $|2\,^2\Sigma_g^+\text{-}8\omega\rangle$, dissociating to the same limit as the $C\,^2\Sigma_u^+$ state, may also contribute in a similar way by accessing population in the $v=0$ level to yield a KER of about 1.6 eV. This pathway, similar to the $|D\,^2\Pi_g\text{-}6\omega\rangle$ pathway, acts to extend the main KER peak to higher energies.

2. High-KER dissociation pathway

We now turn our attention to the unexpected high-KER feature in Fig. 4(b). This peak results from dissociation mechanisms similar to the low-KER peak but involving other pathways with more photon absorption. As more photons are required, this peak is significant only at the higher intensity. Similar to the low-KER peak it involves electronic states leading to the $N^+(^3P)+N(^2D)$ dissociation limit. Additionally, it involves excited states from the next higher manifold leading to dissociation into $N^+(^1D)+N(^2D)$.

A few examples of such highly excited states that lead to high KER, namely, the $|4\,^2\Pi_g\text{-}10\omega\rangle$, $|5\,^2\Sigma_g^+\text{-}12\omega\rangle$, and $|5\,^2\Sigma_u^+\text{-}13\omega\rangle$, are shown in Fig. 5(b). We note, however, that there are a number of other states that similarly can contribute to KER in the observed range but have been omitted from the figure for clarity. The combined contribution from all of these states will yield the broad measured peak centered around 6.1 eV, as shown in Fig. 4(b). Close inspection of Fig. 4(b) also reveals that there are hints of structure in the high-KER peak [48]. This would indeed suggest that more than one pathway is involved in this peak.

Considering the angular distribution [Fig. 4(b)], we again see contributions from both parallel and perpendicular transitions indicating that both $(\Sigma\rightarrow\Sigma)$ and $(\Sigma\rightarrow\Pi)$ transitions are involved. In this case, while the parallel transitions continue to dominate as for the low-KER peak, the relative contribution from perpendicular pathways is larger [see Fig. 4(b)] as the ratio of counts at $|\cos\theta|=0$ to $|\cos\theta|=1$ is larger for KER in the range 4–12 eV than for KER in the range 0–2.5 eV.

It is important to emphasize that the higher KER from dissociation along the pathways shown in Fig. 5(b) is due to the steep part of the repulsive potentials in the vicinity of their crossing with the ground state. Therefore, we find that there are two subsets of groups of PECs that lead to dissociation: low-lying shallow potentials that lead to low KER, and higher-lying steep potentials that lead to high KER in dissociation. The low-lying potentials have a shallow potential well at an internuclear distance R slightly greater than the equilibrium distance (R_0) and cross the highly populated region of the N_2^+ potential well when dressed by 6-8 photons. A few examples of such shallow PECs are shown in Fig. 5(a). The higher-lying potentials are more repulsive and when dressed downwards require more photon absorption to reach the bottom of the N_2^+ potential well than the low-lying shallow potentials. We refer to these states as steeper PECs and a few of them are shown in Fig. 5(b).

The highly excited electronic states associated with the removal of an inner valence electron are steeper than the lower-lying electronic states because of the reduced screening of the nuclear potential. This is made clearer by considering the electronic configurations of N_2 and N_2^+. The ground state of N_2, $X\,^1\Sigma_g^+$, is $(1\sigma_g)^2\,(1\sigma_u)^2\,(2\sigma_g)^2\,(2\sigma_u)^2\,(1\pi_u)^4\,(3\sigma_g)^2$ and that of N_2^+, $X\,^2\Sigma_g^+$, is $[\ldots(1\pi_u)^4(3\sigma_g)^1]$, i.e., to form N_2^+ one electron is removed from the $(3\sigma_g)$ orbital of N_2. When the laser excites a shallow PEC of N_2^+, it is the outer valence electron that is excited. For example, for excitation to the shallow $D\,^2\Pi_g$ state of N_2^+, the electron from the $(3\sigma_g)$ orbital is excited to the $(1\pi_g)$ orbital to result in $[\ldots(1\pi_u)^4(3\sigma_g)^0(1\pi_g)^1]$. However, when the laser excites one of the steeper PECs, it is an inner valence electron that gets excited to an outer orbital, e.g., for excitation of the steep $5\,^2\Sigma_g^+$, state, predominantly a $(2\sigma_g)$ electron is excited to the $(1\pi_g)$ orbital [44,49,50].

Finally, before proceeding, it is interesting to note that the large number of photons required to dissociate N_2^+ (6-13 photons) is reflected in the measured dissociation rates. For example, at 6.0×10^5 W/cm^2 the dissociation rate of N_2^+ is about a factor of 2 lower than O_2^+ under similar ion and laser beam conditions, where for O_2^+ the dominant dissociation paths require 1-4 photons [33]. Likewise, the dissociation rate is approximately a factor of 20 lower than H_2^+ which requires only 1-2 photons to dissociate [51]. Hence one observes directly a link between the large multiphoton nature of the dissociation pathways we have identified and the difficulty in breaking N_2^+ in an intense laser field. We note, given the large difference in the number of photons needed to dissociate, one may have expected an even larger difference in the dissociation rates, although this may be due to the onset of saturation of certain dissociation pathways at this high intensity.

B. Ionization

In addition to dissociation, we have also measured the (1,1) and (1,2) ionization channels of N_2^+. Here we focus on the (1,1) channel that fragments to the $N^+ + N^+$ channel. For

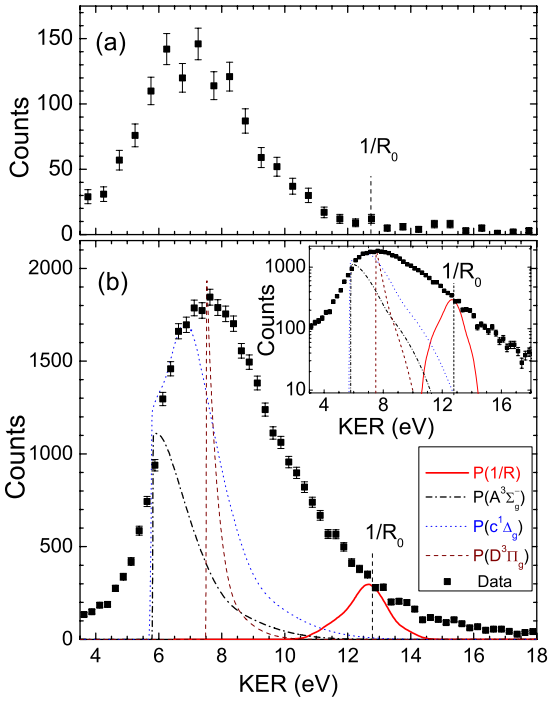

FIG. 6. (Color online) Measured KER distributions for ionization of N_2^+ using 7 fs pulses at intensities (a) 6.5×10^{14} W/cm^2 and (b) 6.0×10^{15} W/cm^2. Note that at higher intensity the KER has a high-energy tail. The error bars denote the statistical error in the data. A sample of computed probability distributions (arbitrary yields) expected for direct ionization to the $c\ ^1\Delta_g$ (dotted curve), $D\ ^3\Pi_g$ (dashed curve), $A\ ^3\Sigma_g^-$ (dash-dotted curve) states of N_2^{2+}, and the Coulomb curve $1/R$ (solid curve) are also shown. The dashed vertical lines (labeled $1/R_0$) indicate the energy corresponding to "Coulomb explosion" of N_2^+ at $R=R_0$.

our measurement of KER at 6.5×10^{14} W/cm^2, shown in Fig. 6(a), we observe a KER peak centered around 7 eV with a width of about 4 eV. The peak of the distribution is comparable to the KER value measured in the majority of studies starting with N_2, using both similar [24] and longer [22,23,25–30] pulse durations.

1. Low-KER ionization pathway

There are two possible mechanisms that could lead to KER in the range of 6–11 eV. The first is what is commonly referred to as direct ionization, and is particularly amenable to the use of short intense pulses [52,53]. Here a wave packet from N_2^+ is launched directly onto the N_2^{2+} manifold of states from where it then dissociates. As a zeroth order approximation, one typically estimates the KER from such a process as given by $1/R_0$ arising from pure Coulomb explosion of the product fragments from the molecule's equilibrium internuclear separation. This energy in the case of N_2^+ is marked by the dashed vertical line labeled $1/R_0$ in Fig. 6(a). The spread of initial internuclear distance $P(R)$ computed using the phase-amplitude method [54] for the vibrational population of the N_2^+ beam at the interaction point [see Fig. 3(b)], results in a KER spread around $1/R_0$ after reflection [55,56] of $P(R)$ onto the $1/R$ Coulomb potential, as shown in Fig. 6(b) by a solid curve. However, in contrast to the transient H_2^{2+} where the $1/R$ Coulomb potential is accurate, the low-lying states of N_2^{2+} have mostly shallow bound-shaped potentials in the direct ionization region [as seen in Fig. 3(a)]. They lie well below the $1/R$ Coulomb curve and would, therefore, yield lower KER than expected for Coulomb explosion.

We have projected the expected N_2^+ vibrational population for the $X\ ^2\Sigma_g^+$ and $A\ ^2\Pi_u$ initial electronic states [given in Fig. 3(b) for the interaction time] onto a few low-lying states of N_2^{2+}, one of which was found to be the most probable by Voss *et al.* [24]. The results of the reflection are shown in Fig. 6(b). It can be seen that this leads to KER values in the 6–11 eV range. One may expect the innermost turning point of the highly excited vibrational states to yield high KER values. However, even the highest vibrational level shown in Fig. 3(b) does not lead to energetic enough breakup. Furthermore, highly excited vibrational states represent a small fraction of the initial vibrational population. It is important to note that the measured KER distribution at the higher intensity (6.0×10^{15} W/cm^2), shown in Fig. 6(b), extends to much higher values than expected for direct ionization.

In addition to direct ionization, however, there is also the possibility of indirect ionization. In this process the molecular wave packet first begins to dissociate along one of the N_2^+ dissociation paths and is then ionized onto the N_2^{2+} states at internuclear distance R larger than R_0. Such a mechanism is usually invoked to explain KER lower than that expected for direct ionization as the ionization step occurs for stretched molecules experiencing a less repulsive potential. Below we will explain the mechanism of indirect ionization by choosing one of the dissociation pathways described earlier.

As we have already identified the likely dissociation pathways, we select the $|2\ ^2\Sigma_g^+\text{-}8\omega\rangle$ state to illustrate one example of a possible indirect ionization pathway. Such a pathway is illustrated in Fig. 7(a) where, in addition to the relevant dressed dissociation states, we dress also the ionization states using the same representation introduced recently to discuss the above-threshold Coulomb explosion of H_2^+ [14]. In Fig. 7(a), a wave packet dissociating on the $|2\ ^2\Sigma_g^+\text{-}8\omega\rangle$ curve may cross onto the dressed $|c\ ^1\Delta_g\text{-}19\omega\rangle$ or $|c\ ^1\Delta_g\text{-}20\omega\rangle$ states at $R=2.4$ a.u. or $R=3$ a.u., respectively, giving KER in the approximate range 6.5–8.5 eV. Here we have not included the $|c\ ^1\Delta_g\text{-}18\omega\rangle$ state because the crossing between the $|c\ ^1\Delta_g\text{-}18\omega\rangle$ and the $|2\ ^2\Sigma_g^+\text{-}8\omega\rangle$ state is at large R such that the electric field of the short laser pulse, used in this experiment, will be weak when the dissociating wave packet reaches the crossing. Also, the $|c\ ^1\Delta_g\text{-}21\omega\rangle$ state is not included because it does not cross the shallower PECs of N_2^+ that give the low KER, however, it crosses the steeper PECs of N_2^+ that result in high KER. As there is a large density of accessible N_2^{2+} states [see Fig. 3(a)] leading to the same $N^+(^3P)+N^+(^3P)$ dissociation limit as the $c\ ^1\Delta_g$ state, each of these may contribute slightly different KER values resulting in a broadening of the observed KER distribution. In addition, as discussed in the introduction, the further the intensity is above the ionization appearance threshold, the more KER broadening incurred.

We have estimated classically the time it takes a dissociating N_2^+ wave packet on the $|2\ ^2\Sigma_g^+\text{-}8\omega\rangle$ state to reach the

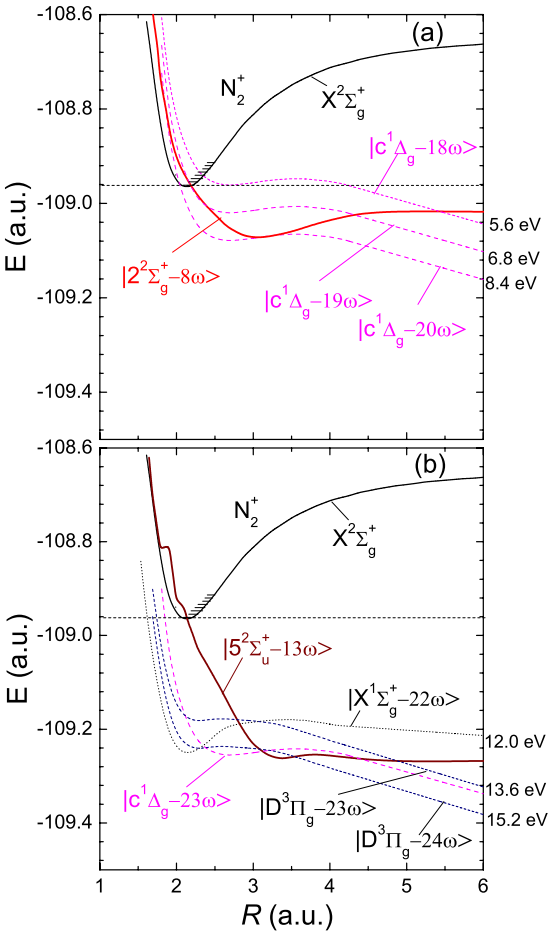

FIG. 7. (Color online) Dressed-states picture of N_2^+ incorporating both dissociation (solid) and ionization (dashed) curves that illustrate the dissociative ionization pathways that lead to (a) low- and (b) high-KER in ionization (see text). Potential energy curves for N_2^+ have been reproduced from Ref. [44]. The structure in some of these curves is due to avoided crossings with neighboring electronic states not shown.

crossing with the $|c\ ^1\Delta_g\text{-}20\omega\rangle$ state of N_2^{2+} at $R\sim3.0$ a.u. and found it to be around 7 fs, which for dissociation initiated on the leading edge of the laser pulse, is within the duration of the pulse. Similarly, the time that it takes for a dissociating wave packet to reach the crossings between the $|2\ ^2\Sigma_g^+\text{-}8\omega\rangle$ state of N_2^+ and some other dressed states of N_2^{2+} at $R\sim2.5-3.0$ a.u. is about 5–7 fs. Thus, both of the aforementioned direct and indirect ionization pathways lead to KER in similar ranges and so we are not able to distinguish here between their contributions.

2. High-KER ionization pathway

In contrast to the low intensity measurement, the KER spectrum for the higher intensity of 6.0×10^{15} W/cm^2 exhibits a much higher KER tail [see Fig. 6(b)]. The fact that the KER distribution extends to higher values than that for low intensities and gets broader with increasing intensity is commonly observed [25]. However, it is surprising that the KER extends well beyond the purely Coulomb explosion energy of 12.8 eV (vertical dashed line, $1/R_0$) and even beyond the whole distribution resulting from the reflection of initial $P(R)$, shown by a solid curve centered around this line. Indeed, the N_2^{2+} states (mostly metastable) are less repulsive than the $1/R$ Coulomb curve for small R, predicting KER below 11 eV. In Fig. 6(b) we have shown a few possible distributions resulting from reflection of the N_2^+ vibrational population [as shown in Fig. 3(b)] onto the N_2^{2+} states, for states resulting in the extreme KER values. Clearly the high energy tail of the distribution extending beyond 11 eV cannot be explained with direct ionization only.

Further insight into the source of the high KER can be found by revisiting the indirect ionization concept. Although typically this has been used to explain lower KER than for direct ionization, as we found from the dissociation spectra, there is a group of extremely steep dissociation curves. Initiating dissociation onto these states, followed then by delayed ionization, can inject energy into the fragments in the first dissociation step. A few examples of such pathways are illustrated in Fig. 7(b). Here we consider dissociation on the steep $|5\ ^2\Sigma_u^+\text{-}13\omega\rangle$ curve. This state first forms a crossing with the dressed $|D\ ^3\Pi_g\text{-}23\omega\rangle$ state of N_2^{2+} at $R=2.7$ a.u., or alternatively with the $|D\ ^3\Pi_g\text{-}24\omega\rangle$ state at $R=3.0$ a.u. The $|c\ ^1\Delta_g\text{-}23\omega\rangle$ state likewise forms a crossing at $R=3.0$ a.u. and the wave packet can end up in the ionization curve by giving up an energy that contributes to the high-KER tail of the energy distribution.

The estimated time for a dissociating N_2^+ wave packet on the $|5\ ^2\Sigma_u^+\text{-}13\omega\rangle$ state to reach the crossing with the $|c\ ^1\Delta_g\text{-}23\omega\rangle$ state of N_2^{2+} at $R=3.0$ a.u. is on the order of 6 fs, which can be considered accessible within the duration of the pulse. For the other crossings around $R=2.7-3.0$ a.u. that are formed between the $|5\ ^2\Sigma_u^+\text{-}13\omega\rangle$ state of N_2^+ and some dressed states of N_2^{2+}, the estimated time is similarly about 5–6 fs.

Each of the pathways discussed above will lead to KER >12 eV, seemingly explaining the origin of the high-KER tail of the distribution in Fig. 6(b). We note that while we have chosen a few specific examples to demonstrate the mechanism responsible for the high-KER tail, there are a number of other similar routes giving a similar range of KER thus preventing the identification of the dominant one.

Finally, we remark on some similarities and differences observed between this experiment on N_2^+ and another recent momentum-imaging experiment on N_2 by Voss *et al.* [24]. At low intensity (10^{14} W/cm^2), notably below the lowest applied here, Voss *et al.* observed the dominant formation path of N_2^{2+} to involve: tunneling single ionization, followed by electron-rescattering excitation to highly excited states of N_2^+, which rapidly tunnel ionize to excited N_2^{2+} prior to decaying. In our experiment such an exotic pathway is immediately negated as, by starting from N_2^+, there is no recolliding electron to excite the N_2^+. In addition, at an intensity in the sequential ionization regime (1.2×10^{15} W/cm^2), Voss *et al.* found that the electron recollision step is replaced by a multiphoton process involving excitation of an inner shell electron, either of neutral N_2 or of the N_2^+ ion. In principle, this excitation process appears similar to the one we observe leading directly to the high-KER peak in N_2^+ dissociation and also responsible for the high-KER in ionization. We note

also the mixed use of terminology between the multiphoton and tunneling descriptions of Voss *et al.* [24]. It is generally accepted that neither regime should be strictly applied exclusively; the multiphoton picture works best for visualizing excitation steps [57] while tunneling is particularly useful to interpret electron-recollision processes [58] or field-enhanced ionization [59,60].

IV. SUMMARY

We have presented the results of dissociation and ionization of N_2^+ in an intense ultrashort laser pulse using a coincidence 3D momentum imaging technique that has allowed us to completely separate the dissociation and ionization channels. We observe a surprising distinct peak in the dissociation with KER values larger than that typically expected for dissociation, which we have assigned to multiphoton excitation to a group of steep PECs from an excited N_2^+ manifold. In turn, indirect ionization following dissociation on these energetic states has led to large kinetic energy release in the $N^+ + N^+$ channel that exceeds the limit of pure Coulomb explosion and the KER expected from direct ionization. While the large density of excited N_2^+ and N_2^{2+} states has not allowed the exact assignment of dissociation pathways for these mechanisms, we wish to convey the counterintuitive concept that ionization of a stretched molecule (i.e., ionization along the dissociation path) can indeed increase the energy released from the system, rather than what is typically observed to decrease it.

ACKNOWLEDGMENTS

The authors wish to thank Professor Z. Chang's group for providing the laser beam and Dr. C. Fehrenbach for his help with the ion beam. This work was supported by the Chemical Sciences, Geosciences, and Biosciences Division, Office of Basic Energy Sciences, Office of Science, U.S. Department of Energy.

[1] K. Codling and L. J. Frasinski, J. Phys. B **26**, 783 (1993).
[2] A. Giusti-Suzor, F. H. Mies, L. F. DiMauro, E. Charron, and B. Yang, J. Phys. B **28**, 309 (1995).
[3] J. H. Posthumus, Rep. Prog. Phys. **67**, 623 (2004), and references therein.
[4] P. H. Bucksbaum, A. Zavriyev, H. G. Muller, and D. W. Schumacher, Phys. Rev. Lett. **64**, 1883 (1990).
[5] G. Jolicard and O. Atabek, Phys. Rev. A **46**, 5845 (1992).
[6] A. D. Bandrauk and M. L. Sink, J. Chem. Phys. **74**, 1110 (1981).
[7] A. Giusti-Suzor, X. He, O. Atabek, and F. H. Mies, Phys. Rev. Lett. **64**, 515 (1990).
[8] A. Zavriyev, P. H. Bucksbaum, J. Squier, and F. Saline, Phys. Rev. Lett. **70**, 1077 (1993).
[9] T. K. Kjeldsen and L. B. Madsen, J. Phys. B **40**, 237 (2007).
[10] D. Zeidler, A. B. Bardon, A. Staudte, D. M. Villeneuve, R. Dörner, and P. B. Corkum, J. Phys. B **39**, L159 (2006).
[11] S. Chelkowski, A. Conjusteau, T. Zuo, and A. D. Bandrauk, Phys. Rev. A **54**, 3235 (1996).
[12] K. Codling, L. J. Frasinski, and P. A. Hatherly, J. Phys. B **21**, L433 (1988).
[13] H. Stapelfeldt, E. Constant, and P. B. Corkum, Phys. Rev. Lett. **74**, 3780 (1995).
[14] B. D. Esry, A. M. Sayler, P. Q. Wang, K. D. Carnes, and I. Ben-Itzhak, Phys. Rev. Lett. **97**, 013003 (2006).
[15] A. Staudte, D. Pavičić, S. Chelkowski, D. Zeidler, M. Meckel, H. Niikura, M. Schöffler, S. Schössler, B. Ulrich, P. P. Rajeev, Th. Weber, T. Jahnke, D. M. Villeneuve, A. D. Bandrauk, C. L. Cocke, P. B. Corkum, and R. Dörner, Phys. Rev. Lett. **98**, 073003 (2007).
[16] J. H. Shirley, Phys. Rev. **138**, B979 (1965).
[17] S.-I. Chu, J. Chem. Phys. **75**, 2215 (1981).
[18] T. F. George, J. Phys. Chem. **86**, 10 (1982).
[19] X. He, O. Atabek, and A. Giusti-Suzor, Phys. Rev. A **38**, 5586 (1988).
[20] G. N. Gibson, L. Fang, and B. Moser, Phys. Rev. A **74**, 041401(R) (2006).
[21] J. H. Posthumus, L. J. Frasinski, A. J. Giles, and K. Codling, J. Phys. B **28**, L349 (1995).
[22] J. H. Posthumus, A. J. Giles, M. R. Thompson, and K. Codling, J. Phys. B **29**, 5811 (1996).
[23] E. Baldit, S. Saugout, and C. Cornaggia, Phys. Rev. A **71**, 021403(R) (2005).
[24] S. Voss, A. S. Alnaser, X.-M. Tong, C. Maharjan, P. Ranitovic, B. Ulrich, B. Shan, Z. Chang, C. D. Lin, and C. L. Cocke, J. Phys. B **37**, 4239 (2004).
[25] J. P. Nibarger, S. V. Menon, and G. N. Gibson, Phys. Rev. A **63**, 053406 (2001).
[26] C. Beylerian and C. Cornaggia, J. Phys. B **37**, L259 (2004).
[27] R. N. Coffee, L. Fang, and G. N. Gibson, Phys. Rev. A **73**, 043417 (2006).
[28] J. McKenna, M. Suresh, B. Srigengan, I. D. Williams, W. A. Bryan, E. M. L. English, S. L. Stebbings, W. R. Newell, I. C. E. Turcu, J. M. Smith, E. J. Divall, C. J. Hooker, A. J. Langley, and J. L. Collier, Phys. Rev. A **73**, 043401 (2006).
[29] S. Banerjee, G. R. Kumar, and D. Mathur, Phys. Rev. A **60**, R25 (1999).
[30] W. Guo, J. Zhu, B. Wang, Y. Wang, and L. Wang, Phys. Rev. A **77**, 033415 (2008).
[31] I. Ben-Itzhak, P. Q. Wang, J. F. Xia, A. M. Sayler, M. A. Smith, J. W. Maseberg, K. D. Carnes, and B. D. Esry, Nucl. Instrum. Methods Phys. Res. B **233**, 56 (2005).
[32] P. Q. Wang, A. M. Sayler, K. D. Carnes, J. F. Xia, M. A. Smith, B. D. Esry, and I. Ben-Itzhak, Phys. Rev. A **74**, 043411 (2006).
[33] A. M. Sayler, P. Q. Wang, K. D. Carnes, B. D. Esry, and I. Ben-Itzhak, Phys. Rev. A **75**, 063420 (2007).
[34] J. McKenna, A. M. Sayler, B. Gaire, N. G. Johnson, E. Parke, K. D. Carnes, B. D. Esry, and I. Ben-Itzhak, Phys. Rev. A **77**, 063422 (2008).
[35] For ionization, information on the momentum of the ejected electron is lost.

[36] P. Hansch and L. D. Van Woerkom, Opt. Lett. **21**, 1286 (1996).
[37] A. M. Sayler, P. Q. Wang, K. D. Carnes, and I. Ben-Itzhak, J. Phys. B **40**, 4367 (2007).
[38] M. Hochlaf, G. Chambaud, and P. Rosmus, J. Phys. B **30**, 4509 (1997).
[39] R. J. Gdanitz, Chem. Phys. Lett. **283**, 253 (1998).
[40] N. Abramzon, R. B. Siegel, and K. Becker, J. Phys. B **32**, L247 (1999).
[41] D. H. Crandall, W. E. Kauppila, R. A. Phaneuf, P. O. Taylor, and G. H. Dunn, Phys. Rev. A **9**, 2545 (1974).
[42] P. C. Cosby, J. Chem. Phys. **98**, 9544 (1993).
[43] A. Ehresmann, L. Werner, S. Klumpp, S. Lucht, H. Schmoranzer, S. Mickat, R. Schill, K.-H. Schartner, Ph. V. Demekhin, M. P. Lemeshko, and V. L. Sukhorukov, J. Phys. B **39**, 283 (2006).
[44] T. Aoto, K. Ito, Y. Hikosaka, A. Shibasaki, R. Hirayama, N. Yamamono, and E. Miyoshi, J. Chem. Phys. **124**, 234306 (2006).
[45] M. Lundqvist, D. Edvardsson, P. Baltzer, and B. Wannberg, J. Phys. B **29**, 1489 (1996).
[46] F. R. Gilmore, R. R. Laher, and P. J. Espy, J. Phys. Chem. Ref. Data **21**, 1005 (1992).
[47] A. Hishikawa, S. Liu, A. Iwasaki, and K. Yamanouchi, J. Chem. Phys. **114**, 9856 (2001).
[48] The structure in the high-KER dissociation peak [Fig. 4(b)] seems to be reproducible when the experiment is repeated under similar conditions.
[49] R. E. Stratmann, G. Bandarage, and R. R. Lucchese, Phys. Rev. A **51**, 3756 (1995).
[50] J. A. Nichols, D. L. Yeager, and P. Jørgensen, J. Chem. Phys. **80**, 293 (1984).
[51] J. McKenna, A. M. Sayler, F. Anis, B. Gaire, N. G. Johnson, E. Parke, J. J. Hua, H. Mashiko, C. M. Nakamura, E. Moon, Z. Chang, K. D. Carnes, B. D. Esry, and I. Ben-Itzhak, Phys. Rev. Lett. **100**, 133001 (2008).
[52] F. Légaré, I. V. Litvinyuk, P. W. Dooley, F. Quéré, A. D. Bandrauk, D. M. Villeneuve, and P. B. Corkum, Phys. Rev. Lett. **91**, 093002 (2003).
[53] A. S. Alnaser, X.-M. Tong, T. Osipov, S. Voss, C. M. Maharjan, P. Ranitovic, B. Ulrich, B. Shan, Z. Chang, C. D. Lin, and C. L. Cocke, Phys. Rev. Lett. **93**, 183202 (2004).
[54] E. Y. Sidky and I. Ben-Itzhak, Phys. Rev. A **60**, 3586 (1999).
[55] H. D. Hagstrum and J. T. Tale, Phys. Rev. **59**, 354 (1941).
[56] C. J. Latimer, Adv. At., Mol., Opt. Phys. **30**, 105 (1992).
[57] J. Rudati, J. L. Chaloupka, P. Agostini, K. C. Kulander, and L. F. DiMauro, Phys. Rev. Lett. **92**, 203001 (2004).
[58] P. B. Corkum, Phys. Rev. Lett. **71**, 1994 (1993).
[59] T. Zuo and A. D. Bandrauk, Phys. Rev. A **52**, R2511 (1995).
[60] T. Seideman, M. Yu. Ivanov, and P. B. Corkum, Phys. Rev. Lett. **75**, 2819 (1995).